Mixing Enhancement in Chemical Lasers, Part II: Theory

Richard J. Driscoll*
Bell Aerospace Textron, Buffalo, New York

Part I of this paper used flow visualization data to construct a phenomenological model for reactant mixing in trip nozzle chemical lasers via a surface stretching mechanism. In Part II this mixing model is used with a two-level laser model to derive scaling laws which describe many of the features observed in trip nozzle data. The mixing model is also used with an aerokinetics code to obtain quantitative predictions of the laser gain; code results are shown to be in good agreement with small-signal gain data.

Nomenclature

C	$= w_O/w_c$
D	= diffusion coefficient
k_c^*	= kinetic collisional deactivation rate, cm^3/(mole-s)
k_c	$= k_c^*[M]$, effective collisional deactivation rate, s^{-1}
K_c	$= k_c/p$
K_d	$= \zeta_d/(pw_O)^2$
$L(t)$	= reactant interface length
L_r	$= L(0)$, reference length; trip jet spacing
p	= cavity pressure, Torr
P	= laser power
$r(t)$	$= y_f(t)L(t)/(w_O L_r)$, fraction of oxidizer reacted
$s(t)$	= strain rate
s_r	$= v_r/(2L_r)$ reference strain rate
t	$= x/u$, flow time
t_d	$= [w_O/(2B_1)]^2/D$, laminar mixing time
t_r	$= w_c/v_r$, reference time
T	= temperature, K
u	= axial velocity, cm/s
v_F, v_O	= fuel and oxidizer stream transverse velocities
v_r	$= v_F + v_O$, reference transverse velocity
w_O, w_F	= oxidizer and fuel nozzle half-width
w_c	= fuel-oxidizer nozzle centerline spacing
x	= axial distance
x_i	$= ut_i$, characteristic distance ($i = b,c,d,e,r$)
$y_f(t)$	= flame location
$\gamma(t)$	$= 2s(t)/k_c$, normalized strain rate
δ^*	$= p\eta$, power flux parameter
ζ	$= xk_c/u$, normalized distance ($\zeta_i = x_i k_c/u$; $i = d,e,r$)
η	= laser efficiency
$\lambda(t)$	$= 2s(t)t_d$, normalized strain rate ($\lambda = \gamma\zeta_d$)
μ	$= (2s_r t_r)^2 = (w_c/L_r)^2$
τ	$= t/t_d = x/x_d$, normalized time ($\tau_i = t_i/t_d$; $i = b,r$)
ψ	$= L(t)/l_r$, normalized surface extension ratio
ψ_r	$= (1+\mu)^{1/2}$, extent of surface stretching
$[M]$	= molar concentration of specie M, moles/cm^3

Subscripts

b	= oxidizer burnout
c	= collisional deactivation
d	= oxidizer burnout (laminar mixing)
e	= end of lasing region
i	= F (fuel nozzle), O (oxidizer nozzle)
r	= reference

Received Nov. 15, 1985; revision received Nov. 17, 1986.

*Group Leader, Laser Fluid Mechanics. Member AIAA.

I. Introduction

DEUTERIUM floride (DF) chemical lasers use gas trip nozzles[1] to accelerate reactant mixing. Gas jets in the tips of the reactant nozzles distort the flow such that the laser power and gain increase by about a factor of two[1,2] when compared with laminar mixing values. Cenkner's data[3] show trip jets do not increase turbulence in the near-nozzle region of the laser cavity. Further, the turbulent laser models of Mirels et al.[4] and Broadwell[5] are unable to explain the scaling of trip nozzle laser data.[1] Thus, there is no evidence which indicates that trip jet mixing is turbulent. Empirical models[2,6,7] are currently used to study trip nozzle flows; however, these models have no physical foundation and are of questionable value in defining laser scaling laws or in predicting the performance of new nozzle designs. The purpose of this paper is to develop the analysis and present results which will validate the surface-stretching trip nozzel mixing model outlined in Ref. 9.

It was suggested[8] that the trip jets cause a distortion and stretching of the reactant interface like that shown in Fig. 1, and that reactant mixing is faster since diffusional mixing occurs along an elongated reactant interface. Experiments[9] have produced flow visualization data showing clear evidence of the surface stretching process; these data were used to develop a model for the surface stretching generation mechanism which could describe the surface stretching rate as a function of reactant nozzle and trip jet geometry. In this paper, the surface stretching model from Ref. 9 is used with the analysis from Ref. 8 to develop scaling laws for trip nozzle laser performance. This surface stretching model is also used with a numerical aerokinetrics code[10] to calculate laser gain distributions which can be compared with data. The analysis results are compared with data to verify the postulated surface stretching mechanism.

II. Scaling Analysis

Flamesheet Combustion Model

The trip jets are believed to stretch the reactant interfaces as shown in Fig. 1. Surface stretching is analyzed by solving the transport equations for an element of the flow in a strain rate field $s(t)$; see Ref. 8, for details. From Ref. 8, the flame location is given by:

$$\frac{dy_f^2}{dt} + 2s(t)y_f^2 = 4B_1^2 D \tag{1}$$

B_1 is a stoichiometry-dependent parameter and D is the laser fuel diffusion coefficient. For laminar mixing, $s(t) = 0$ and $y_f(t) = 2B_1(Dt)^{1/2}$; the oxidizer is fully-reacted when $y_f(t_d) = w_O$ or $t_d = (0.25/D)(w_O/B_1)^2$. D(cm^2/s) scales[11] as $D = ET^{5/3}/p$; E is a composition-dependent coefficient ap-

proximately equal to 0.05 for D_2 fuel and 0.07 for H_2. Nominally $B_1 = 1$ and thus, $t_d = 5pw_O^2/T^{5/3}$. Typical values for p, w_O, and T are 10 Torr, 0.10 cm, and 350 K, respectively, yielding $t_d = 2.88 \times 10^{-5}$ s. For $u = 2.2 \times 10^5$ cm/s, $x_d = 6.3$ cm; this estimate agrees with photographic data[2] which indicate x_d is somewhat greater than 5 cm.

In flows with surface stretching, the element interface length[8] is defined by $L(t)/L_r = \psi(t) = \exp[\int s(t)dt]$, where $L_r = L(0)$. The fraction of the oxidizer reacted is $r(t) = y_f(t)L(t)/(w_O L_r)$ or $r^2(t) = F(t)\psi^2(t)$ where $F(t) = [y_f(t)/w_O]^2$. Writing Eq. (1) in terms of F and $\tau = t/t_d$ yields $dF/d\tau + \lambda(\tau)F = 1$ or, using $r^2 = F\psi^2$, then

$$\frac{dr^2}{d\tau} = \psi^2(\tau) \text{ or } r^2(\tau) = \int_0^\tau \psi^2(\tau)d\tau \tag{2}$$

Eq. (2) defines $r(t)$ for any $s(t)$. Burnout occurs when $r(t_b) = 1$. For laminar mixing, $\psi(t) = 1$ and $t_b = t_d$. For $\psi(t) > 1$, $t_b < t_d$.

Laser Model

A two-level laser model[4] is used to estimate the laser performance. For a unity height semichannel, the molar flow of atomic fluorine is $uw_O[F]$ and the maximum power available is $uw_O[F]\epsilon/2$ (ϵ is the energy per mole of photons). P is the power extracted from the flow and $\eta = 2P \div (uw_O[F]\epsilon)$ is the laser efficiency. For a saturated oscillator with fast kinetic pumping[8]

$$\eta = r(\zeta_e) - \int_0^{\zeta_e} r(\zeta)d\zeta \tag{3}$$

$\zeta = xk_c/u$ is the (flow/collisional deactivation) time scale ratio; $\zeta_e = x_e/x_c$ locates the end of the lasing zone. The effective collisional deactivation rate is $k_c = [M]k_c^*$; $[M]$ is the deactivator concentration and k_c^* is the kinetic rate; $t_c = 1/k_c$ is the deactivation time scale. In DF lasers k_c scales[8] as $k_c = 3.85 \times 10^{10}(X_{HF} + 0.5X_F)pT^{-11/15}$, where X_{HF} and X_F are the hydrogen fluoride and atomic fluorine mole fractions in the laser cavity. For nominal values of $X_{HF} = X_F = 0.06$, $T = 350$ K, and $p = 10$ Torr, then $t_c = 1.14 \times 10^{-5}$ s and $x_c = 2.51$ cm. The (laminar mixing/collisional deactivation) time scale ratio is defined by $\zeta_d = x_d/x_c$; typically, $\zeta_d = 2 - 10$ for high pressure chemical lasers; this implies a low laser efficiency.

Other important scaling parameters are the power per semichannel P and the power flux $\delta = P/w_c$. Using $[F] = X_F P/R_u T$, then $P = [u\epsilon X_F/(2R_u T)](pw_O)$. Write ζ_d as $\zeta_d = K_d(pw_O)^2$ and define $K_p = [u\epsilon X_F/(2R_u T K_d^{1/2})]$. One can then write $P = K_p\zeta_d^{1/2}\eta = K_p P^*$ where $P^* = \eta\zeta_d^{1/2}$. Using $C = w_O/w_c$, then $\delta = CK_p K_d^{1/2} p\eta = CK_p K_d^{1/2}\delta^*$ where $\delta^* = \eta p$. If u, T, and the flow composition are constant, then the laser power and power flux scale as P^* and δ^*.

Two expressions are needed to define ζ_e. When the fluorine is reacted within the lasing zone, $\zeta_e = \zeta_b$ and $r(\zeta_e) = r_e = 1$. If lasing stops before the fluorine has been reacted, $\zeta_e < \zeta_b$ and from Eqs. (2) and (3), $2\zeta_d r_e^2 = \psi_e^2$.

Trip Nozzle Performance Model

Surface stretching is caused by a local lateral motion of the reactants in the trip jet wakes.[9] The trip jets locally block the flow of the nozzle in which they are located, thereby allowing reactants from adjacent nozzles to flow laterally into their wakes. This creates a filament-type structure in the flow with an elongated reactant contact surface (see Fig. 4, Ref. 9). Fuel stream material reaches the oxidizer nozzle centerline at $X_O = uw_O/v_F$ and oxidizer reaches the fuel nozzle centerline at $X_F = uw_F/v_O$. For $x > X_F$ and X_O surface stretching is reduced to a low level due to the interaction between trip jets moving in opposite directions. In general,

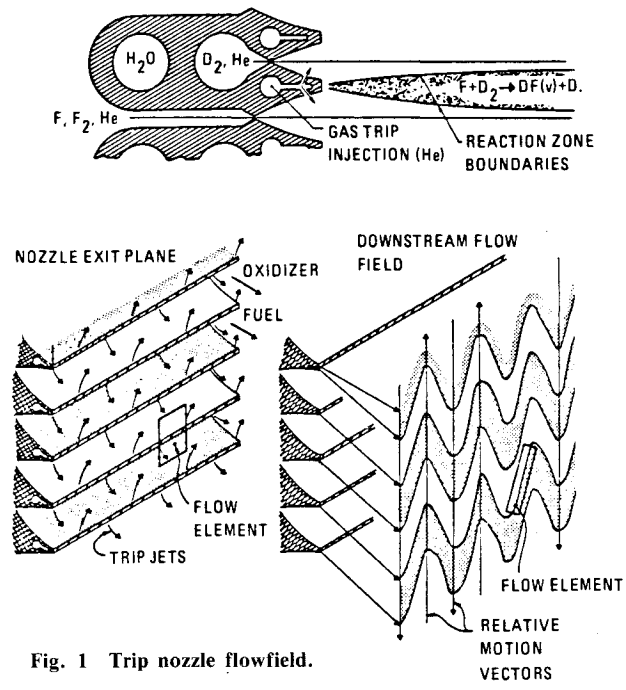

Fig. 1 Trip nozzle flowfield.

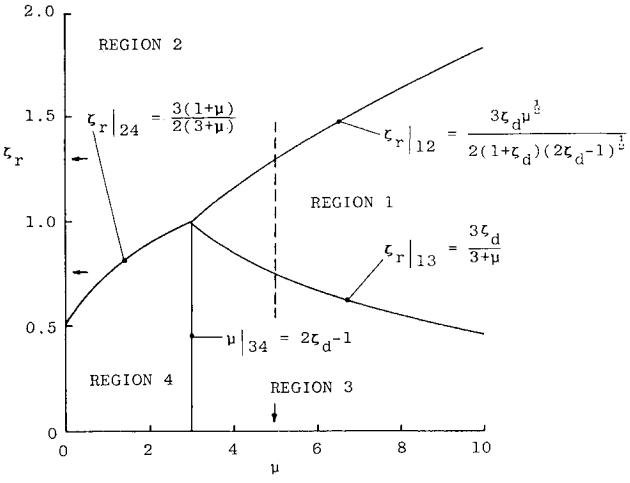

Fig. 2 Laser operational regions ($\zeta_d = 2$).

$X_O > X_F$ and a three-zone strain rate model is needed to describe the surface stretching process; such a model is used in the numerical analysis in Sec. III. A two-zone model is used for the scaling analysis. This model assumes that $X_F = X_O = x_r = ut_r$ and that no surface stretching occurs for $x > x_r$.

Using Eq. (2) from Ref. 9 the extent of surface stretching for the two-zone strain rate model can be written as

$$t \le t_r\colon \psi^2(t) = 1 + (2s_r t)^2 \tag{4a}$$

$$t \ge t_r\colon \psi^2(t) = 1 + (2s_r t_r) = \psi_r^2 = (1+\mu) = \text{const} \tag{4b}$$

$s_r = v_r/(2L_r)$ is the reference strain rate, $v_r = v_F + v_O$ and L_r is the trip jet spacing. Since $\mu = (w_c/L_r)^2$, the extent of surface stretching ψ_r is a function of only the nozzle centerline and trip jet spacing. Substituting Eqs. (4a) and (4b) into Eq. (2) gives the fraction of oxidizer reacted as

$$t \le t_r\colon r^2(\tau) = \tau[1 + \mu(\tau/\tau_r)^2/3] \tag{5a}$$

$$t \ge t_r\colon r^2(\tau) = (1+\mu)\tau - 2\mu\tau_r/3 \tag{5b}$$

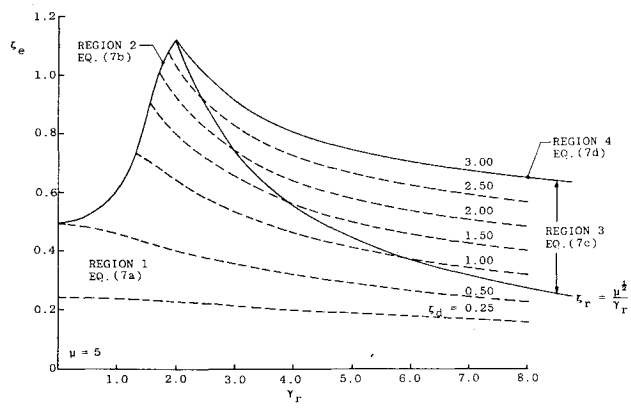

Fig. 3 Lasing zone length ($\mu=5$).

Before Eq. (3) can be used to define η, Eqs. (4) and (5) must be transformed from τ to ζ coordinates using $\tau=\zeta/\zeta_d$ and $\mu=(\gamma_r\zeta_r)^2$. $\gamma_r=2s_r/k_c$ is the (strain/collisional deactivation) rate ratio and $\zeta_r=x_rk_c/\mu$ is normalized suface stretching distance. The resulting equations are:

$$\zeta\le\zeta_r:\ \psi^2(\zeta)=1+(\gamma_r\zeta)^2;\ r^2(\zeta)=\zeta[1+(\gamma_r\zeta)^2/3]/\zeta_d \quad (6a)$$

$$\zeta\ge\zeta_r:\ \psi^2(\zeta)=\psi_r^2;\qquad r^2(\zeta)=[(1+\mu)\zeta-2\mu\zeta_r/3]/\zeta_d \quad (6b)$$

To calculate the laser efficiency using Eq. (3), r_e and ζ_e must be known. Since $\psi(\zeta)$ and $r(\zeta)$ have different forms when $\zeta<\zeta_r$ and $\zeta>\zeta_r$, four equations are needed to define ζ_e over the complete operational range:

Region 1: $\zeta_e=\zeta_b,\ \zeta_e\le\zeta_r$

$$\gamma_r^2\zeta_e^3/3+\zeta_e-\zeta_d=0,\qquad r_e=1 \quad (7a)$$

Region 2: $\zeta_e\le\zeta_b,\ \zeta_e\le\zeta_r$

$$2\gamma_r^2\zeta_e^3/3-\gamma_r^2\zeta_e^2+2\zeta_e-1=0;\qquad r_e^2=2\zeta_e/[\zeta_d(3-2\zeta_e)] \quad (7b)$$

Region 3: $\zeta_e=\zeta_b,\ \zeta_e\ge\zeta_r$

$$\zeta_e=(\zeta_d+2\mu\zeta_r/3)/(1+\mu),\qquad r_e=1 \quad (7c)$$

Region 4: $\zeta_e\le\zeta_b,\ \zeta_e\ge\zeta_r$

$$\zeta_e=\tfrac{1}{2}+2\mu\zeta_r/[3(1+\mu)],\qquad r_e^2=(1+\mu)/(2\zeta_d) \quad (7d)$$

Note that $r(\zeta)$ and ζ_e depend on different parameters when $\zeta_e<\zeta_r$ and $\zeta_e>\zeta_r$. When $\zeta_e<\zeta_r$, surface stretching is an ongoing process and the stretching rate γ_r is the principal parameter. When $\zeta>\zeta_r$ no stretching occurs and the extent of surface stretching $\psi_r=(1+\mu)^{\frac{1}{2}}$ or μ is the principal parameter.

Nominal values for the analysis parameters are given in Table 1. For a typical trip nozzle, $w_c=0.20$ cm, $L_r=0.09$ cm, and the fuel and oxidizer nozzles are approximately equal in size ($w_F=w_O=0.10$ cm). This implies $\mu=4.94$ and $\psi_r=2.44$, i.e., surface stretching will increase the reactant interface length by about 150%. The conditions in Table 1 were obtained from detailed combustor and nozzle calculations on the CL-XI trip nozzle array.[2] The results indicate that the transverse flow angle, surface stretching distance, and strain rate are $\alpha_r=9$ deg, $x_r=0.6$ cm, and $s_r=4\times10^5$ s^{-1}, respectively. This value for x_r falls between the values of $X_F=0.4$ cm and $X_O=0.8$ cm given by the CL-XI data.[2] Typical lasing zone lengths for trip nozzles are $x_e=3$-5 cm; since $x_r<x_e$, the laser is expected to operate as in regions 3 and 4. Table 1 also shows how the parameters vary with flow temperature. Note that ζ_r is small at all temperatures of interest. For a typical value of $T=350$ K, $\zeta_d=2.53$ and $\zeta_r=0.24$.

Figure 2 shows a map of the boundaries between the four operational regions for $\zeta_d=2$, and the expressions derived from Eq. (7) which define the boundaries. All curves intersect when $\zeta_e=\zeta_b=\zeta_r=\zeta_r^*=3\zeta_d/[2(1+\zeta_d)]$; for $\zeta_d=2$, $\zeta_r^*=1.0$. When $\zeta_r>\zeta_r^*$ the laser operates only in regions 1 and 2 where $\zeta_e<\zeta_r$. Since $\zeta_r<0.5$ (see Table 1), Fig. 2 implies that regions 3 and 4 are the most likely operational regions for a trip laser.

Figure 3 shows $\zeta_e(\zeta_r,\zeta_d)$ for $\mu=5$. In regions 2 and 4 ζ_e is not a function of ζ_d. For laminar mixing ($\gamma_r=0$), $\zeta_e<0.5$. From Eq. (7) the maximum value for ζ_e is given by $(\zeta_e)_M=0.5+\mu/(3+\mu)$; for $\mu=5$, $(\zeta_e)_M=1.13$. As $\mu\to\infty$, $(\zeta_e)_M\to1.5$; thus, ζ_e is bounded. For fixed values of μ and ζ_d, as γ_r increases, ζ_e decreases. Equations (7c,d) indicate as $\gamma_r\to\infty$, $\zeta_e\to\zeta_d/(1+\mu)$ in region 3 while $\zeta_e\to0.5$ in region 4; thus, an infinite strain rate does not imply a zero-length lasing zone. The effect of nozzle size on ζ_e can be found from Eq. (7c); multiplying by x_c and going to the limit $\mu\gg1$ indicates that x_e will increase with x_r; since $x_r\sim w_c$, then $x_e\sim w_c$, and the lasing zone lengths will increase with nozzle size. Equation (7d) shows the same trend in region 4. Thus, the model implies that larger nozzles will have longer lasing zones; this is in agreement with available data.

Figure 4 shows $\eta(\gamma_r,\zeta_d)$ for regions 1 and 2 where $\zeta_e<\zeta_r$ and γ_r is the only strain rate parameter. These results were

Table 1 Model parameters

Nozzle geometry	Flow conditions	Strain rate model
$w_c=0.20$ cm	$u=2.20\times10^5$ cm/s	$v_r=6.80\times10^4$ cm/s
$w_O=0.10$ cm	$p=10$ Torr	$\alpha_r=\sin^{-1}(v_r/2u)=8.9$ deg
$L_r=0.09$ cm	$X_{HF}=X_F=0.06$	$x_r=uw_c/v_r=0.59$ cm
$\mu=(w_c/L_r)^2=4.94$	$E=0.05$ (D_2)	$s_r=v_r/(2L_r)=3.78\times10^5$ s^{-1}
$\psi_r=(1+\mu)^{\frac{1}{2}}=2.44$	$B_1=1$	

Temperature dependent parameters

Temperature, K	250	300	350	400	450
$t_d=(4EB_1^2)^{-1}pw_O^2T^{-5/3}\times10^5$ s	5.04	3.72	2.88	2.30	1.89
$x_d=ut_d$ cm	11.09	8.18	6.34	5.06	4.16
$k_c=3.85\times10^{14}(X_{HF}+0.5X_F)pT^{-11/5}$ s^{-1}	18.38	12.30	8.77	6.53	5.04
$t_c=k_c^{-1}\times10^5$ s	0.54	0.81	1.14	1.53	1.98
$x_c=ut_c$ cm	1.19	1.78	2.51	3.37	4.36
$\zeta_d=x_d/x_c$	9.32	4.60	2.53	1.50	0.95
$\zeta_r=x_r/x_c$	0.50	0.33	0.24	0.18	0.14
$\lambda_r=2s_rt_d$	38.10	28.12	21.77	17.39	14.29
$\gamma_r=2s_rt_c$	4.08	6.12	8.62	11.57	14.97
$K_c=k_c/p\times10^{-3}$, (s-Torr)$^{-1}$	18.38	12.30	8.77	6.53	5.04
$K_d=\zeta_d/(pw_O)^2$, (Torr-cm)$^{-2}$	9.32	4.60	2.53	1.50	0.95

obtained using Eqs. (3) and (6a) and they show that η increases as ζ_d decreases and γ_r increases. The laminar solution ($\gamma_r=0$) for $\zeta_d=2.0$ gives $\eta=0.33$ while for $\gamma_r=4$, $\eta=0.68$. Thus, even moderate values of γ_r are seen to significantly increase.

In regions 3 and 4 where $\zeta_e>\zeta_r$, the integral in Eq. (3) must be evaluated in two parts. Using Eqs. (6a) and (6b), η can be rewritten as

$$\eta=r_e-\frac{1}{\zeta_d^{1/2}}\int_0^{\zeta_r}\left(\zeta+\frac{1}{3}\gamma_r^2\zeta^3\right)^{1/2}d\zeta$$
$$-\frac{1}{\zeta_d^{1/2}}\int_{\zeta_r}^{\zeta_e}\left[(1+\mu)\zeta-\frac{2}{3}\mu\zeta_r\right]^{1/2}d\zeta \qquad (8)$$

The first integral in Eq. (8) can be written as $2\zeta_r^{3/2}I(\mu)/3$ where

$$I(\mu)=\frac{3}{2}\int_0^1\left(\zeta_1+\frac{1}{3}\mu\zeta_1^3\right)^{1/2}d\zeta_1 \qquad (9)$$

The second integral can be evaluated analytically and Eq. (8) is written as

$$\eta=r_e-\frac{2}{3}\zeta_d\left[\frac{r_e^3}{1+\mu}+\left(\frac{\zeta_r}{\zeta_d}\right)^{3/2}\right]f(\mu) \qquad (10)$$

where $f(\mu)=I(\mu)-(1+\mu/3)^{3/2}/(1+\mu)$. Figure 5 shows $I(\mu)$ and $f(\mu)$ and indicates that $f(\mu)\approx 0.60$ for $\mu=3$–10, e.g., for $\mu=5$, $f(\mu)=0.57$.

In region 3 $r_e=1$ while in region 4 $r_e=[(1+\mu)/(2\zeta_d)]^{1/2}$; substituting into Eq. (10) and rearranging terms gives

Region 3 ($\zeta_e=\zeta_b$):

$$\eta=1-\frac{2\zeta_d}{3(1+\mu)}\left[1+\left(\frac{\zeta_r}{\zeta_d}\right)^{3/2}(1+\mu)f(\mu)\right] \qquad (11a)$$

Region 4 ($\zeta_e\le\zeta_b$):

$$\eta=\frac{1}{3}\left[\frac{2(1+\mu)}{\zeta_d}\right]^{1/2}\left[1-\left(\frac{2}{1+\mu}\right)^{1/2}\zeta_r^{3/2}f(\mu)\right] \qquad (11b)$$

Equations (11a) and (11b) and the results in Fig. 4 for regions 1 and 2 were used to construct Fig. 6 which shows how η varies with μ and ζ_r for $\zeta_d=2$. For laminar mixing $\gamma_r=0$, $\zeta_r\to\infty$, and $\eta=0.33$. The highest laser efficiencies occur in region 3 when $\zeta_r=0$, i.e., all surface stretching occurs instantaneously at the nozzle exit plane. For a fixed value of μ, η increases as ζ_r decreases, however, when ζ_r is small the increase in η is minimal, e.g., for $\mu=5$, decreasing ζ_r from 0.46 to zero increases η from 0.69 to 0.78, a 13% gain. Since $\zeta_r<0.50$ for a typical trip nozzle (see Table 1), little would be gained by changing nozzle designs to decrease ζ_r further.

For $\zeta_r\to 0$, Eqs. (11a) and (11b) reduce to the following form:

Region 3 ($\zeta_e=\zeta_b$):

$$\eta=1-\frac{2}{3}\left(\frac{\zeta_d}{\psi_r^2}\right) \qquad (12a)$$

Region 4 ($\zeta_e\le\zeta_b$):

$$\eta=\frac{2^{1/2}}{3}\left(\frac{\psi_r^2}{\zeta_d}\right)^{1/2} \qquad (12b)$$

when $\psi_r=1$, Eqs. (12a) and (12b) reduces to the laminar mixing solution of Ref. 4. Equations (12a) and (12b) can be reduced to laminar mixing form by writing ζ_d in terms of an effective diffusivity $D_e=\psi_r^2 D$. Thus, when ζ_r is small, surface stretching can be modeled using laminar mixing solutions with the diffusion coefficient increased by ψ_r^2. Since $\psi_r^2=1+(w_c/L_r)^2$, D_e is a function of the nozzle and trip jet geometry.

Jet Penetration Effects

Equations (11) and (12) presume that the trip jets penetrate to the nozzle centerlines and the surface stretching stops after a time $t_r=w_c/v_r$. In practice, the trip jet penetration h_j can be varied continuously by changing the jet mass flow rate. Let $H=h_{jF}+h_{jO}$ represent the total trip jet span where h_{jF} and h_{jO} are the fuel and oxidizer trip jet penetration distances, respectively. For any H, the time duration of the surface stretching process is $t_r=H/v_r$ and from Eq. (4) the extent of surface stretching is $\psi_r=[1+(H/L_r)^2]^{1/2}$. For $H=0$, $\psi_r=1$, and the laminar mixing results are recovered. As trip jet penetration increases, then H and ψ_r increase with a consequent increase in the laser efficiency, e.g., see Eq. (12). Thus, the surface stretching model formulation can describe laser scaling with trip jet penetration. Since the extent of surface stretching depends on the sum of the fuel and oxidizer trip jet penetrations, the model also explains the experimental observation that it is more effective to have trip jets in both the fuel and the oxidizer nozzles rather than in only one.

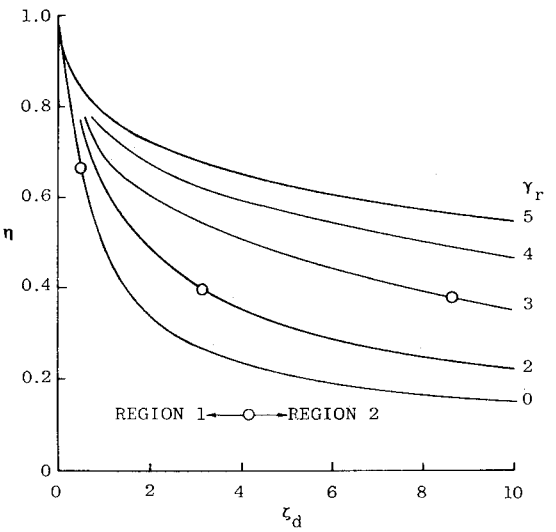

Fig. 4 Laser efficiency in regions 1 and 2.

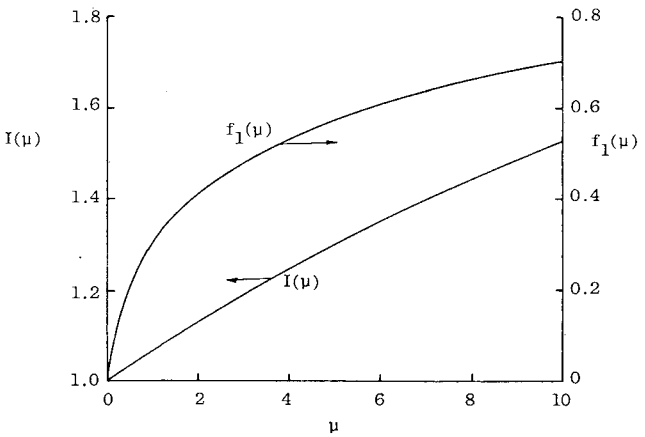

Fig. 5 Surface stretching functions $I(\mu)$ and $f(\mu)$.

Scaling Laws

Scaling laws describing the effect of p, w_c, L_r, and v_r on η and δ^* can be derived from Eq. (11). Let $\zeta_d = K_d(pw_O)^2 = C^2K_d(pL_r)^2\mu$, $k_c = K_c p$, and $\zeta_r = w_c k_c / v_r = K_c(pL_r)^{1/2}/v_r$ where K_d and K_c are composition and temperature dependent coefficients (see Table 1). Substituting into Eqs. (11a) and (11b) yields

Region 3:

$$\eta = 1 - \frac{2}{3} C^2 K_d (pL_r)^2 \left(\frac{\mu}{1+\mu}\right) - \frac{2}{3}\left[\frac{K_c^3(pL_r)}{C^2K_d v_r^3}\right]^{1/2} \mu^{1/4} f(\mu) \quad (13a)$$

$$= 1 - 0.422(pL_r)^2\left(\frac{\mu}{1+\mu}\right) - 0.0388(pL_r)^{1/2}\mu^{1/4} f(\mu) \quad (13b)$$

Region 4:

$$\eta = \frac{(2/K_d)^{1/2}}{3C(pL_r)}\left(\frac{1+\mu}{\mu}\right)^{1/2} - \frac{2}{3}\left[\frac{K_c^3(pL_r)}{C^2K_d v_r^3}\right]^{1/2}\mu^{1/4} f(\mu) \quad (13c)$$

$$= \frac{0.593}{(pL_r)}\left(\frac{1+\mu}{\mu}\right)^{1/2} - 0.0388(pL_r)^{1/2}\mu^{1/4} f(\mu) \quad (13d)$$

The results in Eqs. (13b) and (13d) are for $T = 350$ K and the parameter values in Table 1; these equations are used in the examples which follow. The last term in Eqs. (13a) and (13d) is called the strain rate term since it is the only one which depends on the surface stretching rate; it is the same in regions 3 and 4 and is the only one which depends on v_r. This term goes to zero as $v_r \to \infty$ and in this limit Eq. (13) reduced to Eq. (12), implying that all surface stretching occurs instantaneously at the nozzle exit plane. Under typical conditions the strain rate term should have only a second order effect on η so long as $v_r \gg K_c$. Assume $v_r = 10K_c$ is required; since $K_c = 0(10^4)$ and $v_r \approx 2v_F \approx 2v_O$, this suggests that the laser nozzles be designed to should produce transverse velocities of at least 5×10^4 cm/s.

Figure 7 shows how the efficiency and power flux parameter vary with p and μ. These results were obtained using Eqs. (13b) and (13d) and are for a fixed value of $L_r = 0.09$ cm. Since L_r is constant and $\mu = (w_c/L_r)^2$, the different values of μ reflect changes in the nozzle size w_c; Eq. (13) was written specifically as shown to consolidate all variations of the nozzle scale w_c within the parameter μ. The laminar mixing results shown in Fig. 7 were obtained using Eqs. (12a) and (12b) with $\psi_r = 1$ and $w_O = Cw_c = CL_r\mu^{1/2} = 0.10$ cm (since $L_r = 0.09$ cm = constant and $\mu = 5$ was the value chosen for comparison purposes). The circled points in Fig. 7 mark the regions 3-4 boundary.

Figure 7 shows that η decreases with increasing cavity pressure for all values of μ with the laminar mixing curve falling much faster than those for the trip nozzle. In region 3 where $\zeta_e = \zeta_b$, δ^* increases rapidly with increasing p; in

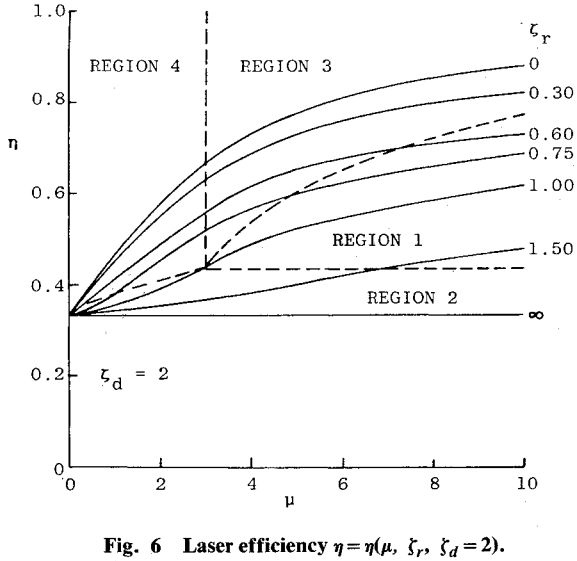

Fig. 6 Laser efficiency $\eta = \eta(\mu, \zeta_r, \zeta_d = 2)$.

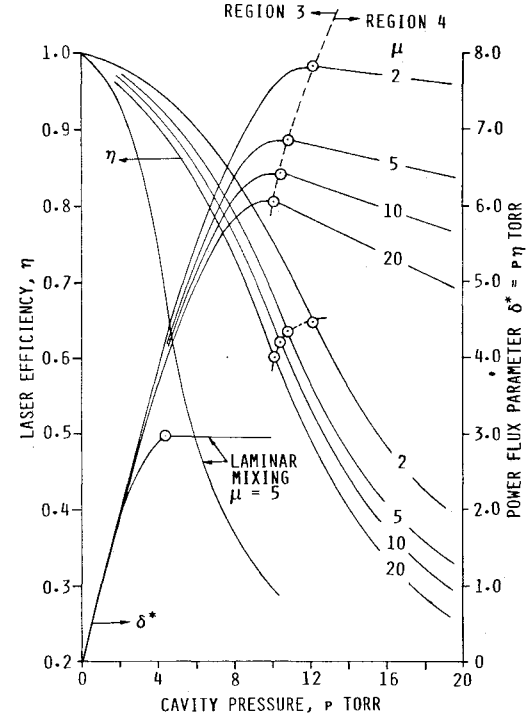

Fig. 7 Scaling of efficiency η and power flux δ^* with cavity pressure p and nozzle size μ.

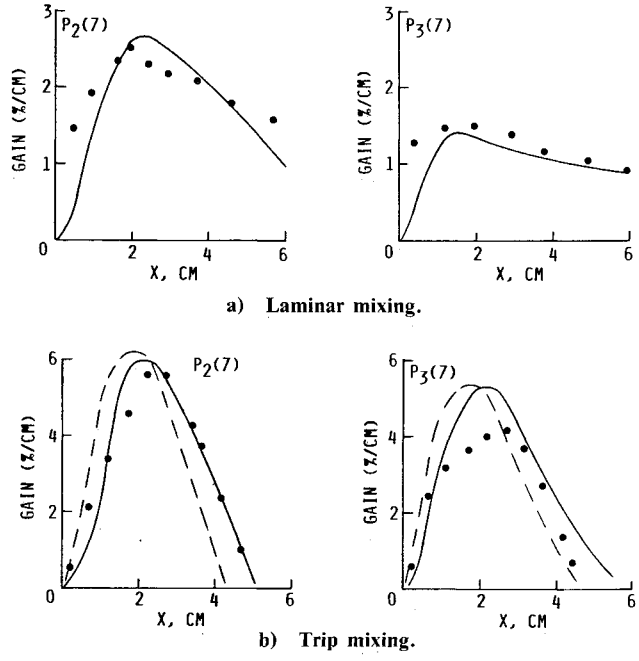

Fig. 8 Comparison of CL-XI small signal gain data (•) for $P_2(7)$ and $P_3(7)$ lines with surface stretching model (——) results from BLAZE-II aerokinetics code; (15, 30) test conditions. DCM model (- - -) results for $\psi_r = 2.30$, DCM = $\psi_r^2 = 5.29$.

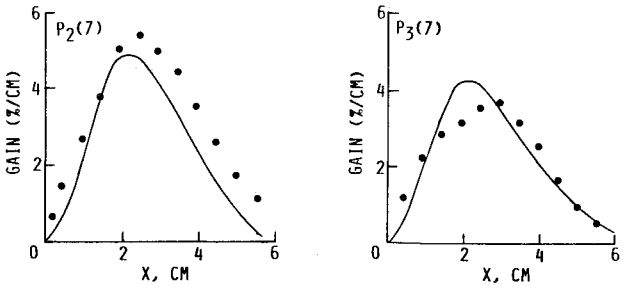

a) (15, 40) test condition.

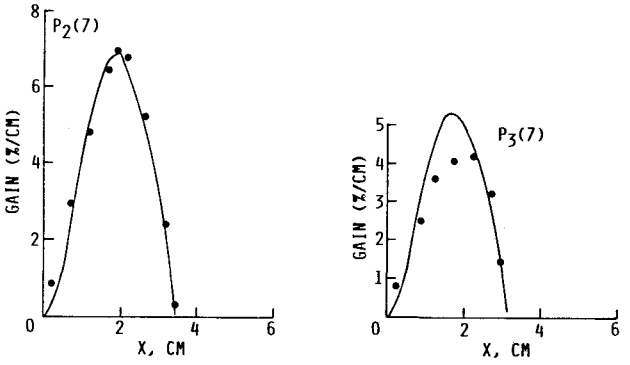

b) (10, 30) test condition.

Fig. 9 Comparison of CL-XI small-signal gain data (•) for $P_2(7)$ and $P_3(7)$ lines with surface stretching model (——) results from BLAZE-II aerokinetics code.

region 4 where $\zeta_e < \zeta_b$, δ^* is independent of p for laminar mixing and decreases slowly with increasing p for the trip nozzles due to the effect of the strain rate term. For any μ the power flux has a maximum at the junction point between regions 3 and 4. At this junction point $\zeta_d = \psi_r^2/2$ (see Fig. 3); using $\zeta_d = C^2 K_d (pL_r)^2 \mu$, then the cavity pressure at this junction point (the critical pressure p_c) can be written as

$$p_c = \frac{\psi_r}{(2K_d)^{1/2} w_O} = \frac{1}{(2K_d)^{1/2} CL_r} \left(\frac{1+\mu}{\mu}\right)^{1/2} \tag{14}$$

Consider the first equation given for p_c. For laminar mixing ($\psi_r = 1$), $p_c \sim w_O^{-1}$; an equivalent statement of this condition is $\zeta_d = 1/2$ (a result first given by Mirels et al.[4]). For a fixed nozzle size, then $p_c \sim \psi_r$, i.e., p_c increases linearly with the extent of surface stretching. For the laminar mixing nozzle with $\mu = 5$, Eq. (14) gives $p_c = 4.5$ Torr ($K_d = 2.53$, see Table 1) while for the corresponding trip nozzle with $\psi_r = 2.44$, $p_c = 10.9$ Torr; thus, surface stretching increases the critical pressure. The second form of Eq. (14) indicates that p_c is relatively insensitive to μ and, therefore, to the nozzle size w_c, e.g., for $\mu = 2$–20, $p_c = 12.1$–10.1 Torr. Critical pressures for trip nozzles are, therefore, expected to be in the 10–12 Torr range and insensitive to the nozzle size; this is to be contrasted with laminar and turbulent mixing results[4,5] which indicate $p_c \sim w_O^{-1}$.

The results in Fig. 7 indicate that $p < 3$ Torr diffusional mixing is sufficiently fast that mixing enhancement is not needed. The superiority of trip nozzles at high cavity pressures ($p > 5$ Torr) is obvious, e.g., for $\mu = 5$ and $p = 10$ Torr, the trip nozzle values for η and δ^* are a factor of 2.3 larger than for the corresponding laminar mixing nozzle. This factor of two improvement predicted by the surface stretching model is in agreement with available data[1] from trip nozzles.

Wilson[1] indicates that trip nozzle δ^* is relatively insensitive to changes in the nozzle scale w_c; laminar and turbulent models,[4,5] in contrast, show a strong sensitivity, e.g., $\delta^* \sim w_c^{-1}$. In Fig. 7, changes in w_c are described by μ. The results indicate that for any cavity pressure p both η and δ^* decrease slowly as μ increases, e.g., increasing μ from 5 to 20 (a factor of two in w_c) decreases the maximum value of δ^* from 6.86 to 6.05, i.e., by 12%. Thus, the model shows the nozzle power flux is not strongly dependent on nozzle size, in agreement with Wilson's data.[2]

III. Aerokinetics Model

Simple models like those in Sec. II are useful for deriving laser scaling laws and data correlations[12]; however, they cannot accurately describe the laser gain distributions. Such results must be obtained from aerokinetics codes which solve the flowfield conservation equations using a detailed set of chemical kinetic rates to describe the laser pumping, energy transfer, and deactivation processes.

A streamtube aerokinetics code was used for analysis herein; detailed descriptions of this type of code can be found in Refs. 7 and 10. These codes model the flowfield using three streamtubes which contain fuel, oxidizer, or a fuel/oxidizer mixture (see Fig. 1). Chemical reactions occur and lasing species exist only in the mixed flow streamtube. The axial variation of the mixed flow properties is obtained by solving the appropriate conservation equations. Currently, these models assume the reactant interface length L_r is constant and that the mass addition rate into the mixed flow streamtube is $dm_i/dt = (\rho u)_i L_r d\Delta_i/dt$ where Δ_i represents the mixing layer penetration into the fuel and oxidizer streams. To use this formulation in a flow with surface stretching, one need only define an equivalent mixing layer width which accounts for the increase in the reactant interface length. Equation (2) defines a mixing layer width $\Delta_i(t)$ when the stoichiometry constant B_1 is replaced by an equivalent mixing parameter K_m. One can, therefore, use Eq. (2) to derive the following mixing layer growth law for flows with surface stretching:

$$\frac{d\Delta_i^2}{dt} = 4K_m^2 D_i \psi^2(t) \tag{15}$$

Surface stretching affects Δ_i through the surface extension ratio $\psi(t)$. When $\psi(t) = 1$, the laminar mixing law is recovered.

The BLAZE-II[10] aerokinetics code was modified to use Eq. (15) and subsequently, to calculate the small-signal gain distributions for the CL-XI gas trip laser; the results were then compared with data for a number of different lasing lines and flow conditions. A three-level DF laser model with a kinetic rate package composed of 41 reactions (pumping, deactivation, and $V-V$ exchange) was used to calculate specie concentrations. Detailed combustor and nozzle calculations were made to define the cavity inlet flow properties and surface stretching parameters. The gain calculations were found to be quite sensitive to the nozzle wall temperture and atomic fluorine mass fraction, and the cavity boundary condition. The nozzle parameters affect the specie mass flux profiles across the laser nozzle, and, therefore, the rate at which reactants enter the mixed flow streamtube. The cavity boundary condition affects the cavity pressure distribution. All results herein are for a wall temperature of 500 K, no atomic fluorine at the wall, and a constant area cavity boundary condition over $x = 0$–2 cm with a small area increase thereafter. Varying these parameters could always improve the agreement between model and data for any one data set; the above values, however, gave good agreement for all data examined and were used for all calculations.

The model was compared with gain data for a laminar mixing case and three trip flow conditions at different diluent levels. The oxidizer and fuel stream diluent levels are β_O and β_F where β_i is the molar ratio of helium to atomic fluorine; the three conditions examined were $(\beta_O, \beta_F) = (10,$

30), (15, 30), and (15, 40). All tests were at a total mass flux of about 2.0 g/s/cm^2. Figure 8 shows a comparison of model and data for the $P_2(7)$ and $P_3(7)$ lasing transitions for the (15, 30) test condition for both laminar and trip mixing. The laminar mixing data were modeled using $K_m = 1.0$ and K_m was fixed at this value for the remainder of the study. For the trip mixing case $\psi(t)$ was calculated using the three-zone strain rate model described in Ref. 9 [see Eqs. (3-5)]; the strain rate model parameters for this test condition are $s_r = 3.8 \times 10^5$ s^{-1}, $X_F = 0.43$ cm, and $X_O = 0.88$ cm. The residual strain rate parameter ϵ was set at 1%, implying little reactant surface stretching for $x > X_O$. The results in Fig. 8 show that the model is in reasonably good agreement with the (15, 30) data for both the laminar and trip mixing tests. Similar results are shown in Fig. 9 for the (10, 30) and (15, 40) diluent level test conditions and again, the agreement is satisfactory. It is important to note that there are no adjustable parameters in the surface stretching mixing model; all the parameters which are used in defining $\psi(t)$ are calculated from the flow condition and laser nozzle geometry.

Equation (15) indicates that the effective diffusion coefficient in a flow with surface stretching is $D_{ei} = D_i \psi^2(t)$. If the surface stretching distance is short compared to the lasing zone length, then $\psi(t) = \psi_r$ over most of the lasing zone and consequently, $D_{ei} = D_i \psi_r^2$; surface stretching, in effect, increases the diffusion coefficient by a constant factor of ψ_r^2. The approach of using a laminar mixing model with a constant diffusion coefficient multiplier (DCM) has had limited success in modeling trip nozzle data[2,6] and the surface stretching model outlined herein provides some justification for this approach. For the test condition shown in Fig. 8b, $\psi_r = 2.30$ which implies a diffusion coefficient multiplier (DCM) of 5.29. The dashed lines in Fig. 8b show the results from a DCM = 5.29 model calculation; the model predicts the correct gain level but the gain peak is too close to the nozzle. Better results are obtained if a DCM somewhat less than ψ_r^2 is used. The surface stretching model indicates that the DCM is a function of the nozzle and trip jet geometry, and this result has been verified in modeling studies using data from different size nozzles.

IV. Summary and Conclusions

The mechanism for the fast mixing observed in trip nozzle chemical lasers was postulated[8] to be a stretching of the fuel-oxidizer interface and a model for this process relating the surface stretching parameters to the nozzle and trip jet geometry was proposed in Ref. 9. In this paper, this model was used in both a scaling analysis and a numerical aerokinetics code to obtain results which could be compared with data. The aerokinetics code results for the gain distributions are shown in Figs. 8 and 9 and they compare favorably with data for both laminar and trip mixing conditions. The scaling analysis results are qualitative, however, they are consistent with the observed characteristics of trip nozzle lasers; in particular, they indicate that: 1) trip jet mixing will not increase laser efficiency at low cavity pressures since diffusional mixing is sufficiently fast at this condition; 2) at high cavity pressures, trip jet mixing will more than double laser power output; 3) laser efficiency will increase with trip jet penetration; 4) when the trip jets penetrate to the nozzle centerlines, the laser efficiency and power flux are relatively insensitive to changes in the reactant nozzle sizes; 5) the principal parameter influencing the laser efficiency is the extent of surface stretching ψ_r rather than the strain rate γ_r; 6) the critical cavity pressure which defines the maximum power increases with ψ_r and is in the range of 10–12 Torr for trip nozzle lasers; 7) the surface stretching model reduces to a laminar mixing form with an enhanced diffusion coefficient when the surface stretching distance is small compared to the lasing zone length; 8) the laminar model DCM is ψ_r^2 and is a function of the nozzle width and trip jet spacing. The results given above support the conclusion that the physical mechanism for trip jet mixing is surface stretching and that the model given in Ref. 9 provides an adequate first order description of this process.

References

[1]Wilson, L. E., "Deuterium Fluoride CW Chemical Layers," *Journal de Physique*, Colloque C9, Vol. 41, Nov. 1980, pp. C9.1-C9.8. (See also AIAA Paper No. 76-344 with the same title by L. E. Wilson and D. L. Hook.)

[2]Driscoll, R. J. and Tregay, G. W., "Flowfield Experiments on a DF Chemical Laser," *AIAA Journal*, Vol. 21, Feb. 1983, pp. 241-246.

[3]Cenkner, A. A., "Laser Doppler Velocimeter Measurements on Supersonic Mixing Nozzles that Employ Gas Trips," *AIAA Journal*, Vol. 20, March 1982, pp. 383-389.

[4]Mirels, H., Hofland, R., and King, W. S., "Simplified Model of CW Diffusion-Type Chemical Laser, *AIAA Journal*, Vol. 11, Feb. 1973, pp. 156-164.

[5]Broadwell, J. E., "Effect of Mixing Rate on HF Chemical Laser Performance," *Applied Optics*, Vol. 13, April 1974, pp. 962-967.

[6]O'Keefe, D., Sugimura, T., Behrens, W., Bullock, D., and Dee, D., "Comparison of LAMP and BLAZER Code Calculations with TRW CL-XV Measurements," *Optical Engineering*, Vol. 18, July 1979, pp. 363-369.

[7]Yang, T. T., "Modeling of CW Chemical Laser with Annular Unstable Resonator," *AIAA Journal*, Vol. 18, Oct. 1980, pp. 1223-1232.

[8]Driscoll, R. J., "The Effect of Reactant-Surface Stretching on Chemical Laser Performance," *AIAA Journal*, Vol. 22, Jan. 1984, pp. 65-74.

[9]Driscoll, R. J., "Mixing Enhancement in Chemical Lasers. Part I: Experiments," *AIAA Journal*, Vol. 24, July 1986, pp. 1120-1126.

[10]Zelazny, S. W., Driscoll, R. J., Raymonda, J. W., Blauer, J. A., and Solomon, W. C., "Modeling DF/HF CW Lasers: An Examination of Key Assumptions," *AIAA Journal*, Vol. 16, April 1978, pp. 297-304.

[11]Fristrom, R. M. and Westenberg, A. A., *Flame Structure*, McGraw Hill, New York, 1965, p. 276.

[12]Gross, R. W. F. and Bott, J. F., eds., *Handbook of Chemical Lasers*, Wiley, New York, 1976, pp. 345-387.